

Distributed Hammerstein modeling for cross-coupling effect of multi-axis piezoelectric micropositioning stages

Hai-Tao Zhang, *Senior Member, IEEE*, Bo Hu, Linlin Li, Zhiyong Chen, *Senior Member, IEEE*, Dongrui Wu, *Senior Member, IEEE*, Bowen Xu, Xiang Huang, Guoying Gu, *Member, IEEE* and Ye Yuan, *Member, IEEE*

Abstract—Hysteresis modeling is interesting yet challenging for piezoelectric actuated systems, which are often used in micro/nano scale measurement and manufacturing equipments. However, due to its complexity, few efforts have been devoted to characterizing cross-coupling hysteresis effect of multi-axis piezoelectric micropositioning stages. To this end, a distributed Hammerstein model, composed of a cascaded connection of a static nonlinearity and a dynamic linearity, is proposed in this paper to approximate the nonlinear spatial/temporal cross-coupling effect. This model outperforms conventional piezo models such as the Preisach model. Meanwhile, theoretical analysis is provided to guarantee the convergence of the proposed Hammerstein model. Finally, extensive experiments are conducted to verify the superiority of the proposed modeling method.

Index Terms—Piezoelectric devices, hysteresis, modeling

I. INTRODUCTION

These years have witnessed the tremendous development of nano-positioning systems widely used in modern nanometer measurement and manufacturing equipments. To obtain high precision of nano-scale positioning systems like scanning tunneling microscopes (STMs) [1], atomic force microscopes (AFMs) [2], lithographic machines [3], ultrahigh vacuum precise positioning devices [4], micro-robot arm [5], etc., smart material actuators, represented by piezoelectric actuators [6], [7], [8] are commonly used.

The positioning control precision of piezoelectric actuators is bottlenecked by the nonlinear dynamics including creep and hysteresis. Recently, the adverse effects of cross-couplings of multi-axis piezoelectric micropositioning stages have attracted more and more attentions [9]. Take AFMs for example, *triangular signals* applied to the X -piezoelectric actuated scanner often deform the trajectory in the X - Y landscape and hence distorts the scanned images due to the X - Y axes cross-coupling effect [10]. Significantly, the cross-coupling effect

is dominant at high frequencies, which may cause not only crumpling and tilting the scans [10], [11] but also the loss of the surface information about the sample [12]. Such a non-negligible cross-coupling effect mainly caused by inter-axis friction, pressure and pre-load forces substantially lowers the positioning control precision. Thus, the cross-coupling effect becomes one of the main complications associated to micro/nano scale detection processes (e.g., AFMs and STMs) and nano-manufacturing equipments (e.g., lithographic machines). However, due to its complex cross-axis dynamics, most of the existing modeling schemes, including Preisach [13], Bouc-Wen [14], Prandtl-Ishlinskii [15], cascaded nonlinearity [6] models, merely focus on the single-axis hysteresis dynamics.

Till date, there are very few niche modeling methods for cross-coupling hysteresis of the multi-axis piezoelectric micropositioning stages, which are however indispensable for both piezoelectric actuated mechanism analysis and high-precision controller design. Most of the existing works [9], [11], [16], [17] focused on decoupling the cross-couplings to facilitate controller design. For instance, Yong *et al.* [9] developed a robust H_∞ controller to minimize the X - Y axes cross-coupling of the piezoelectric actuated stage of an AFM. Habibullah *et al.* [11] designed an internal reference model-based optimal linear quadratic Gaussian (LQG) controller to address the cross-coupling effect of a high-precision lateral positioning used in a piezoelectric tube scanner (PTS) of an AFM. Wu *et al.* [16] proposed an adaptive double integral sliding mode control scheme to compensate for the cross-coupling in AFMs, where phase feedback signals were used as well to increase the scanning sensitivity. Rana *et al.* [17] designed a multi-input multi-output model predictive control (MPC) method to counteract the cross-coupling in a PTS.

Among the few existing works of direct identification on cross-coupling hysteresis dynamics, Tan *et al.* [18] developed a neural-network-based sandwich model to describe the nonlinear X - Y axes interactive dynamics, which was afterwards used in a nonlinear decoupling controller to counterbalance the cross-axis coupling effect. Based on the response surface methodology, Qin *et al.* [19] proposed a computational optimization method to address the cross-axis interactive dynamics. With such an optimization method, they presented a novel mechanical design for a 2-DOF piezoelectric actuator to substantially alleviate the cross-axis coupling. With the assistance of laser interferometry sensors, Bhagat *et al.* [20] proposed a parameter identification approach, which was afterwards

This work was supported by the National Natural Science Foundation of China (NNSFC) under Grants with Nos. U1713203, 51729501, 61673189, 51535004 and 61751303. (Corresponding author: Y. Yuan)

H.-T. Zhang, B. Hu, B. Xu, X. Huang, D. Wu and Y. Yuan are with the School of Automation, the State Key Lab of Digital Manufacturing Equipment and Technology, and the Key Lab of Imaging Processing and Intelligence Control, Huazhong University of Science and Technology, Wuhan 430074, China (email: yye@hust.edu.cn).

L. Li and G. Gu are with the State Key Laboratory of Mechanical System and Vibration, School of Mechanical Engineering, Shanghai Jiao Tong University, Shanghai 200240, China.

Z. Chen is with the School of Electrical Engineering and Computing, The University of Newcastle, Callaghan, NSW 2308, Australia.

used in a robust motional controller to compensate for the cross-axis coupling effect between the two axes of a flexure-based stage. Fung *et al.* [21] proposed an improved Bouc-Wen hysteresis model to identify the cross-coupling effects, where a real-coded genetic algorithm method was adopted to train the model parameters. Das *et al.* [22] provided a linear data-driven modeling method to approach the cross-coupling dynamics of a scanner in the lateral and longitudinal axes, which was subsequently used in a negative-imaginary damping controller to restrain the first resonant mode and to attenuate the cross-coupling effect as well. Xu [23] proposed a least square support vector machine learning method, which has gained better modeling performance than traditional Bouc-Wen model [14]. From the modeling aspect of distributed parameter systems, Qi *et al.* [24] proposed a kernel-based modeling scheme with the assistance of Karhunen-Loève decomposition and Galerkin method, which shows the potential of approaching cross-coupling effect of piezoelectrical stage. Li *et al.* [25] and Lai *et al.*[26] adopted a finite element analysis method to investigate the cross-coupling dynamics around the resonance frequency. Accordingly, they designed a center-thickened beam structure together with a symmetric configuration of the parallelogram flexure to effectively reduce the cross-coupling effect. So far, most of the existing cross-coupling modeling methods are either linear or lumping system orientation. Thus, it is still an urgent yet challenging task to develop an effective modeling method to approximate the nonlinear spatial/temporal dynamics of cross-coupling effect of piezoelectric stages.

To fulfill such a task, in this paper, we develop a pure data-driven distributed multi-channel Hammerstein model. The present model is a cascade connection of a static nonlinear block and a dynamic spatial/temporal linear block. By feeding a periodical exciting signal to the Y -axis, the spatial/temporal data is gathered at different X - Y axes contacting positions. Accordingly, a multi-channel identification scheme is derived to guarantee high modeling precision without any prior-knowledge about the mid-output. Afterwards, matrix spectrum analysis is conducted to guarantee the convergence and the modeling accuracy of the proposed Hammerstein modeling method. Finally, data-driven experimental modeling performances are provided to verify the effectiveness and superiority of the model.

The remainder of the paper is organized as follows. The piezoelectric actuated stage is described in Section II. Then, the distributed Hammerstein modeling scheme is proposed in Section III, and a systematic analysis on the convergence of the scheme is provided as well. Afterwards, extensive modeling experiments are conducted to verify the feasibility and superiority of the proposed Hammerstein model in Section IV. Finally, the conclusion is drawn in Section V.

Throughout the paper, the following notations are used: A^T denotes the transposition of a matrix A , \mathbb{R} , \mathbb{R}^+ , \mathbb{Z} , \mathbb{N} and \mathbb{C} are real number, positive real number, integers, positive integers and complex number sets, respectively. The operator \otimes represents the Kronecker product.

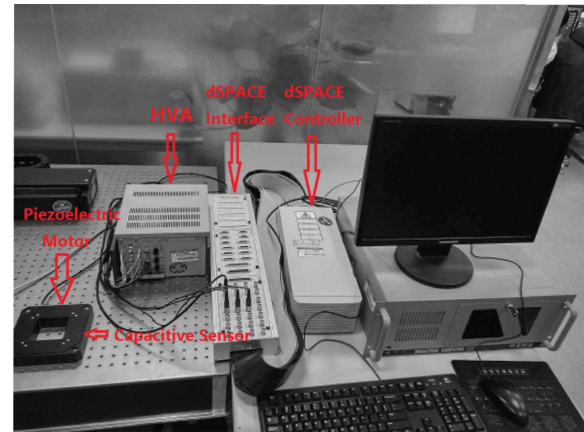


Fig. 1. The Physik Instrument (P-563.3CD) two-axis piezoelectric actuated stage.

II. EXPERIMENTAL PIEZOELECTRIC ACTUATED STAGE

The experimental platform, i.e., a Physik Instrument (PI-563.3CD) two-axis piezoelectric actuated stage (in abbr. PI stage) is shown in Fig. 1 with structure given in Fig. 2. Therein, two piezoelectric actuators and two capacitive position sensors are mounted to the X - and Y -axes, respectively. The resonance frequencies of X - and Y - axes are both 140Hz. The block diagram of the PI stage is given in Fig. 3, where an exciting signal u is fed into a high-voltage amplifier (HVA) via a digital-to-analog (D/A) converter, where a u_c signal is yielded to drive the PI stage. Then, the X - and Y -axes displacements are measured by capacitive displacement transducers (CDTs). Afterwards, the displacement signal is transferred to a voltage signal and then fed into the dSPACE-DS1103 block through an analog-to-digital (A/D) converter.

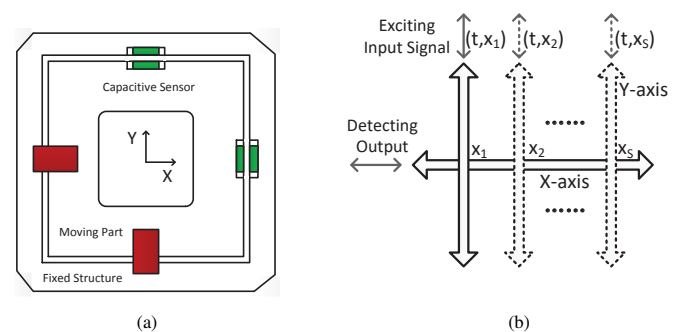


Fig. 2. (a): Schematic map of the piezoelectric stage; (b): Cross-coupling between X - Y axis of different X - Y axes contacting positions.

In Fig. 2(a), due to the pre-load forces together with the frictions and the asymmetrical structure of the PI-stage, the motions along X - and Y -axes affect each other, which is thus named as the cross-coupling effect. Quantitative analysis confirms that the intensity of cross-coupling is non-negligible for high-precision positioning control scenarios. To investigate such a complex coupling effect, we feed an exciting signal u to Y -axis of the PI-stage at different X - Y axes contacting positions x_i , $i = 1, \dots, S$, and measure the X -axis

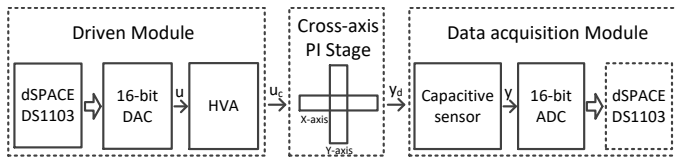


Fig. 3. The block diagram of the PI-stage control system.

displacement as shown in Fig. 2(b). Distinct cross-couplings are observed at different contacting positions, which induces the non-negligible adverse spatial/temporal effect of the cross-couplings.

III. MODELING METHOD DEVELOPMENT

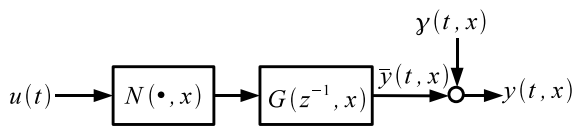


Fig. 4. Distributed Hammerstein model.

In this section, we aim to develop a nonlinear Hammerstein model to approximate the spatial/temporal cross-axis dynamics. As shown in Fig. 4, suppose the desired dynamics consists of a cascade connection of a memoryless nonlinearity $N(\cdot, x)$ and a distributed linear block $G(z^{-1}, x)$. More specifically, they are governed by the following the input-output equation

$$y(t, x) = G(z^{-1}, x) \cdot N(u(t), x) + \gamma(t, x), \quad (1)$$

where $u(t), y(t, x), \gamma(t, x) \in \mathbb{R}$ are the system input, output and external noise, respectively. The output function $y(t, x)$ represents the X -axis displacement at t when the X - Y axes contacting position is x , as shown in Fig. 2(b).

Firstly, the linear block is assumed to be expanded by a rational orthonormal basis series as follows

$$G(z^{-1}, x) = \sum_{i=1}^m \rho^T(x) \xi_i L_i(z^{-1}) = [L(z^{-1}) \otimes \rho(x)]^T \xi \quad (2)$$

where $\xi = [\xi_1^T, \dots, \xi_m^T]^T$ and $L(\cdot) = [L_1(\cdot)^T, \dots, L_m(\cdot)^T]^T$, and $L_1(z^{-1}), \dots, L_m(z^{-1})$ form a rational orthonormal basis on the Hardy space $\mathbb{H}(\mathbf{T})$ [27]. For our model, they are set as discrete Laguerre series detailed in Appendix. The term $\rho^T(x) \xi_i \in \mathbb{R}$, $i = 1, 2, \dots, m$, is the associated coefficient depending on the spatial position x . Specifically, $\rho(\cdot) : \mathbb{R} \mapsto \mathbb{R}^q$ is a known vector function and $\xi_i \in \mathbb{R}^q$ a vector parameter to be identified.

Secondly, the nonlinear block can be described as

$$N(u(t), x) = \sum_{i=1}^n \psi^T(x) \eta_i g_i(u(t)) = [g(u(t)) \otimes \psi(x)]^T \eta, \quad (3)$$

where $\eta = [\eta_1^T, \dots, \eta_n^T]^T$, $g(\cdot) = [g_1(\cdot)^T, \dots, g_n(\cdot)^T]^T$, $g_i(\cdot) : \mathbb{R} \mapsto \mathbb{R}$ is a known nonlinear basis function and $\psi^T(x) \eta_i \in \mathbb{R}$ is its associated coefficient depending on the spatial position x , $i = 1, \dots, n$. Specifically, $\psi(\cdot) : \mathbb{R} \mapsto \mathbb{R}^p$ is a known vector

function and $\eta_i \in \mathbb{R}^p$ a vector parameter to be identified. Generally speaking, $g_i(\cdot)$ can be chosen as polynomials, radial basis functions (RBF), wavelets, etc. For simplicity, we pick $g_i(\cdot)$ as the polynomial series in our model. Both the functions $\rho(\cdot)$ and $\psi(\cdot)$ can be selected as some basis functions, e.g., polynomials, Jacobies, trigonometric functions, or their combinations.

By Eqs. (2) and (3), Eq. (1) is equivalent to

$$y(t, x) = [L(z^{-1}) \otimes \rho(x)]^T \xi \cdot [g(u(t)) \otimes \psi(x)]^T \eta + \gamma(t, x). \quad (4)$$

Direct calculation leads to

$$\begin{aligned} & [L(z^{-1}) \otimes \rho(x)]^T \xi \cdot [g(u(t)) \otimes \psi(x)]^T \eta \\ &= [L(z^{-1}) \otimes \rho(x)]^T \otimes [g(u(t)) \otimes \psi(x)]^T [\xi \otimes \eta] \\ &= [L(z^{-1}) \otimes \rho(x) \otimes g(u(t)) \otimes \psi(x)]^T [\xi \otimes \eta], \end{aligned}$$

thus Eq. (4) is equivalent to

$$y(t, x) = \phi^T(z^{-1}, u(t), x) \theta + \gamma(t, x). \quad (5)$$

where

$$\phi(z^{-1}, u(t), x) = L(z^{-1}) \otimes \rho(x) \otimes g(u(t)) \otimes \psi(x)$$

is a known vector function and

$$\theta = \xi \otimes \eta$$

is a vector parameter to be identified. For convenience, we denote the noise-free output as

$$\bar{y}(t, x) = \phi^T(z^{-1}, u(t), x) \theta. \quad (6)$$

Next, the modeling procedure is to establish an equation

$$\hat{y}(t, x) = \phi^T(z^{-1}, u(t), x) \hat{\theta} \quad (7)$$

where $\hat{\theta} = \hat{\xi} \otimes \hat{\eta}$ is a valid estimation of θ for some vectors $\hat{\xi}$ and $\hat{\eta}$. This objective is usually impossible when noise appears, so a more realistic model is

$$\hat{y}(t, x) = \phi^T(z^{-1}, u(t), x) \sum_{i=1}^{N_c} \hat{\theta}^{(i)}, \quad \hat{\theta}^{(i)} = \hat{\xi}^{(i)} \otimes \hat{\eta}^{(i)} \quad (8)$$

for an integer $N_c \geq 1$. By using the similar arguments, the model (8) is equivalent to

$$\begin{aligned} \hat{y}(t, x) &= \sum_{i=1}^{N_c} \hat{G}(z^{-1}, x) \cdot \hat{N}(u(t), x), \\ \hat{G}^{(i)}(z^{-1}, x) &= [L(z^{-1}) \otimes \rho(x)]^T \hat{\xi}^{(i)}, \\ \hat{N}^{(i)}(u(t), x) &= [g(u(t)) \otimes \psi(x)]^T \hat{\eta}^{(i)}. \end{aligned} \quad (9)$$

Such a model is called a *multi-channel Hammerstein model* and N_c is the number of channels. The objective of this paper is: *using the given input $u(t)$ with position x and the measured output $y(t, x)$ from Eq. (5) (or equivalently Eq. (1)), find valid estimation $\hat{\theta}^{(i)} = \hat{\xi}^{(i)} \otimes \hat{\eta}^{(i)}$, $i = 1, \dots, N_c$, such that the output $\hat{y}(t, x)$ determined by the multi-channel Hammerstein (8) (or equivalently (9)) matches $\bar{y}(t, x)$ of (6) in a certain sense.*

The approach to achieving the aforementioned objective is developed in a rigorous manner as follows. Select an input series $U := [u(t_1), u(t_2), \dots, u(t_N)]$ with temporal variable sequence $\{t_1, t_2, \dots, t_N\}$, and collect the corresponding NS -sampling output spatial/temporal dataset with spatial variable

sequence $X := [x_1, x_2, \dots, x_S]$ for two integers $N, S \geq 1$. Thus, the dynamics (5) become

$$Y = \Phi\theta + \Upsilon \quad (10)$$

with

$$\begin{aligned} Y &:= [y(t_1, x_1), y(t_2, x_1), \dots, y(t_N, x_1), \dots, \\ &\quad y(t_1, x_S), y(t_2, x_S), \dots, y(t_N, x_S)]^T, \\ \Phi &:= [\phi(z^{-1}, u(t_1), x_1), \dots, \phi(z^{-1}, u(t_N), x_1), \dots, \\ &\quad \phi(z^{-1}, u(t_1), x_S), \dots, \phi(z^{-1}, u(t_N), x_S)]^T, \\ \Upsilon &:= [\gamma(t_1, x_1), \gamma(t_2, x_1), \dots, \gamma(t_N, x_1), \dots, \\ &\quad \gamma(t_1, x_S), \gamma(t_2, x_S), \dots, \gamma(t_N, x_S)]^T. \end{aligned}$$

Then two steps are applied: (i) find a valid estimation $\hat{\theta}$ of θ through the data Φ and Y , depending on U and X ; and (ii) derive the multiple channel estimation $\hat{\theta}^{(i)} = \hat{\xi}^{(i)} \otimes \hat{\eta}^{(i)}$, $i = 1, \dots, N_c$, from $\hat{\theta}$ to fit in the multi-channel Hammerstein model (8).

To elaborate the two steps, we first define a function $\mathcal{C}(\cdot)$ such that

$$\hat{\Theta} = \mathcal{C}^{-1}(\hat{\theta}) \in \mathbb{R}^{np \times mq}, \quad \hat{\theta} = \mathcal{C}(\hat{\Theta}) \in \mathbb{R}^{npmq}$$

where the vector $\hat{\theta}$ is the block column matrix of $\hat{\Theta}$, i.e., stacking the block column of $\hat{\Theta}$ on the top of each other. Then, we give a result on the singular value decomposition (SVD) of a matrix with rank deficiency.

Theorem 3.1: (Theorem 2.5.3 [28]) Let the singular value decomposition (SVD) of the matrix $\hat{\Theta} \in \mathbb{R}^{s_1 \times s_2}$ with $\text{rank}(\hat{\Theta}) = k \geq 1$ be given as $\hat{\Theta} = W\Sigma V^T$ where

$$\begin{aligned} W &= [w_1, \dots, w_{s_1}] \in \mathbb{R}^{s_1 \times s_1}, \\ V &= [v_1, \dots, v_{s_2}] \in \mathbb{R}^{s_2 \times s_2} \end{aligned} \quad (11)$$

are orthogonal matrix and

$$\begin{aligned} \Sigma &= \text{diag}\{\sigma_1, \dots, \sigma_s\} \in \mathbb{R}^{s_1 \times s_2}, \quad s = \min\{s_1, s_2\} \\ \sigma_1 &\geq \sigma_2 \geq \dots \geq \sigma_k > \sigma_{k+1} = \dots = \sigma_s = 0. \end{aligned}$$

Then, for $0 \leq l \leq k$,

$$e^{(l)} := \left\| \hat{\Theta} - \sum_{i=1}^l \sigma_i w_i v_i^T \right\|_2 = \sigma_{l+1}.$$

N.B. if $k = s$, we denote $\sigma_{s+1} = 0$ for the completeness of notation.

The main technical result is stated in the following theorem.

Theorem 3.2: For the distributed system (1), given the input data $U = [u(t_1), u(t_2), \dots, u(t_N)]$ and the sampling positions $X = [x_1, x_2, \dots, x_S]$, the following three assumptions hold:

- There exist integers $N, S > 1$, such that Φ and Y (see Eq. (10)) obey the dynamics (5);
- For an arbitrary $\epsilon_1 > 0$, an estimation $\hat{\theta}$ for θ exists such that $\|\hat{\theta} - \theta\| \leq \epsilon_1$;
- For an arbitrary $\epsilon_2 > 0$, the matrix $\hat{\Theta} = \mathcal{C}^{-1}(\hat{\theta})$ has an SVD given in Theorem 3.1 such that $e^{(N_c)} \leq \frac{1}{mq} \epsilon_2$ with $N_c \leq k$;

Then, the output $\hat{y}(t, x)$ given by Eq. (8) with

$$\begin{aligned} \hat{\eta}^{(i)} &= w_i, \\ \hat{\xi}^{(i)} &= \sigma_i v_i, \quad i = 1, \dots, N_c, \end{aligned} \quad (12)$$

approaches $\bar{y}(t, x)$ of Eq. (6) in the sense of

$$\|\hat{y}(t, x) - \bar{y}(t, x)\| \leq \|\phi(z^{-1}, u(t), x)\| \epsilon \quad (13)$$

for $\epsilon = \epsilon_1 + \epsilon_2$.

Proof: Denote

$$\vartheta := \hat{\theta} - \sum_{i=1}^{N_c} \hat{\xi}^{(i)} \otimes \hat{\eta}^{(i)}$$

and

$$\vartheta = [\vartheta_1^T, \vartheta_2^T, \dots, \vartheta_{mq}^T]^T \in \mathbb{R}^{npmq}, \quad \vartheta_i \in \mathbb{R}^{np}.$$

From the definition of $\mathcal{C}(\cdot)$, one has

$$\begin{aligned} \mathcal{C}^{-1}(\vartheta) &= \mathcal{C}^{-1}(\hat{\theta}) - \sum_{i=1}^{N_c} \mathcal{C}^{-1}(\hat{\xi}^{(i)} \otimes \hat{\eta}^{(i)}) \\ &= \hat{\Theta} - \sum_{i=1}^{N_c} \hat{\eta}^{(i)} (\hat{\xi}^{(i)})^T = \hat{\Theta} - \sum_{i=1}^{N_c} \sigma_i w_i v_i^T \end{aligned}$$

and hence

$$\|\mathcal{C}^{-1}(\vartheta)\| = e^{\langle N_c \rangle} \leq \frac{1}{mq} \epsilon_2.$$

By the definition of a matrix norm,

$$\begin{aligned} \|\mathcal{C}^{-1}(\vartheta)\| &= \sup_{x \neq 0, x \in \mathbb{R}^{mq}} \frac{\|\mathcal{C}^{-1}(\vartheta)x\|}{\|x\|} \\ &= \sup_{x \neq 0, x \in \mathbb{R}^{mq}} \frac{\|[\vartheta_1, \vartheta_2, \dots, \vartheta_{mq}]x\|}{\|x\|} \\ &\geq \|\vartheta_i\|, \quad \forall i = 1, \dots, mq, \end{aligned}$$

which implies

$$\|\vartheta\| = \sum_{i=1}^{mq} \|\vartheta_i\| \leq mq \|\mathcal{C}^{-1}(\vartheta)\| \leq \epsilon_2.$$

Next, it is ready to calculate that

$$\begin{aligned} &\|\hat{y}(t, x) - \bar{y}(t, x)\| \\ &= \left\| \phi^T(z^{-1}, u(t), x) \left(\sum_{i=1}^{N_c} \hat{\xi}^{(i)} \otimes \hat{\eta}^{(i)} - \theta \right) \right\| \\ &\leq \|\phi^T(z^{-1}, u(t), x)\| \left\| \sum_{i=1}^{N_c} \hat{\xi}^{(i)} \otimes \hat{\eta}^{(i)} - \hat{\theta} + \hat{\theta} - \theta \right\| \\ &\leq \|\phi^T(z^{-1}, u(t), x)\| (\|\vartheta\| + \|\hat{\theta} - \theta\|) \\ &\leq \|\phi^T(z^{-1}, u(t), x)\| (\epsilon_1 + \epsilon_2). \end{aligned}$$

The proof is thus completed. \blacksquare

To achieve a valid estimation $\hat{\theta}$ for θ , we can use least square estimate (LSE) method [29] as follow

$$\hat{\theta} = (\Phi^T \Phi)^{-1} \Phi^T Y = \Phi^+ Y, \quad (14)$$

provided that the inverse $(\Phi^T \Phi)^{-1}$ exists. The LSE approach can almost guarantee a sufficiently small estimation error ϵ_1 in Theorem 3.2. The parameter N_c represents the number of Hammerstein channels. The larger N_c , the smaller $\epsilon_2 = e^{\langle N_c \rangle} = \sigma_{N_c+1}$ can be selected due to the monotonic order

of σ_i . In particular, if $N_c = k$, one can pick $\epsilon_2 = 0$. These observations are summarized in the following corollary.

Corollary 3.1: *Let $\hat{\theta}$ calculated by Eq. (14) be the LSE of θ in the model (5). Suppose the model (8) (or (9)) is given with Eq. (12) for $N_c = k$, and $\hat{\Theta} = C^{-1}(\hat{\theta})$ has an SVD given in Theorem 3.1. Assume $\|\phi(z^{-1}, u(t), x)\|$ is bounded and the noise $\gamma(t, x)$ is independent of the system input $u(t)$. Then, for any $\varepsilon > 0$, there exist integers $N, S \geq 1$ such that,*

$$\|\hat{y}(t, x) - \bar{y}(t, x)\| \leq \varepsilon, \quad (15)$$

with probability of one; denoted as

$$\hat{y}(t, x) \xrightarrow{a.s.} \bar{y}(t, x). \quad (16)$$

Proof: Let $a \geq 0$ as the bound of $\|\phi(z^{-1}, u(t), x)\|$ and $\epsilon_1 = \varepsilon/a$. Since the external noise $\gamma(t, x)$ is independent of the persistent exciting bounded regressor $\phi(z^{-1}, u(t), x)$, the LSE $\hat{\theta}$ satisfies $\hat{\theta} \xrightarrow{a.s.} \theta$ [29]. That is, there exist integers $N, S \geq 1$ such that,

$$\|\hat{\theta} - \theta\| \leq \epsilon_1, \quad (17)$$

with probability of one. As $N_c = k$, one has $\epsilon_2 = mqe^{(N_c)} = 0$ according to the SVD in Theorem 3.1. As a result of Theorem 3.2, one has

$$\|\hat{y}(t, x) - \bar{y}(t, x)\| \leq a(\epsilon_1 + \epsilon_2) = \varepsilon, \quad (18)$$

also with probability of one. ■

Remark 3.1: When $L_i(z^{-1})$ is selected as a stable transfer function, the position x and the input $u(t)$ are bounded, and the functions $\rho_i(x)$, $g_i(u)$, and $\psi_i(x)$ are all bounded, one has a bounded $\|\phi(z^{-1}, u(t), x)\| = \|L(z^{-1}) \otimes \rho(x) \otimes g(u(t)) \otimes \psi(x)\|$.

Remark 3.2: Theorem 3.2 and Corollary 3.1 provide the convergence conditions for the proposed modeling method (14) and (12). By the analysis in Theorem 3.2, the spatial variable x should appear in both the linear block $G(z^{-1}, \cdot)$ and the nonlinear block $N(\cdot)$ of the distributed Hammerstein model, otherwise the convergence and optimality of the present Hammerstein modeling method can not be guaranteed. This claim will also be verified by extensive data-driven modeling experiments of cross-couplings on the PI-stage afterwards. Note that Theorem 3.2 holds even in the presence of colored external noises $\gamma(t, x)$, if only it is independent of the input signal $u(t)$. By Theorem 3.2, the required identification channel number (i.e., $\text{rank}(\hat{\Theta}) = k$) can be determined in advance. But sampling data length should be obtained by applications.

Remark 3.3: The SVD calculation for the proposed multi-channel Hammerstein model is more time consuming than the pseudo inversion calculation of Preisach model. Accordingly, the convergence time of the former is longer than the latter, but has higher precision, which is beneficial to reduce the positioning control error of multi-axis piezoelectric stages.

Remark 3.4: In the low frequency, typically the linear dynamics part of a piezoelectric system is the DC gain, and the multi-value effect is due to the hysteresis nonlinearity. However, in this work, we present an alternative method to capture the coupled hysteresis and dynamics of piezoelectric actuators with a Hammerstein model. One of the benefits of this development is that the complex hysteresis model is avoided. In this way, both the static nonlinearity and the linear dynamics of the Hammerstein model contribute to describe the hysteresis.

Remark 3.5: Although the cascaded architectures can effectively reduce the X - Y coupling effect, the present parallel architecture in Fig. 2 is irreplaceable due to the following advantages. i) the runout is easily measured and corrected [30]; ii) if both axes have the same mechanical bandwidth (like the present case), the testing direction can be chosen arbitrarily [31]. So, it makes sense to investigate the coupling effects. Note that the main contribution of this work lies in the modeling of the coupling effects. Based on our previous control efforts [32], [33] on Hammerstein models, the present work can be expected to extend to controller design. Meanwhile, it is observed from extensive experiments that, the cross-coupling caused by inter-axis friction, pressure and pre-load forces have larger effects at lower exciting frequencies.

IV. MODELING EXPERIMENTS

First, the PI stage is fed with a periodical exciting voltage signal of $u(t) = 4 + 5\sin(2\pi ft)$ V with frequency $f \in \{1, 5, 10, \dots, 130\}$ Hz. It is used to describe periodical exciting signals often encountered in real applications. For each integral value of exciting frequency f , we sample NS response signal sequence $y(t, x)$ with $t \in \{t_1, t_2, \dots, t_S\}$, $S = 6000$; $x \in \{x_1, x_2, \dots, x_N\} = \{0, 30, \dots, 240\}$ μ m, $N = 9$. Distinct evolution curves of cross-coupling effect are shown in Fig. 5 at different contacting positions x_i , $i = 1, \dots, N$, along increasing exciting frequency f . It is observed that the cross-coupling effect varies at different contacting positions and exciting frequencies. More precisely, the averages of the cross-coupling effect percentage at $f \in \{1, 10, 35, 100\}$ Hz are 0.30%, 0.33%, 0.99%, and 6.34%, respectively, which are non-negligible for high-precision positioning scenarios. Meanwhile, the cross-coupling effect is intensified along increasing exciting frequency.

In the present distributed multi-channel Hammerstein model (9), the parameters are picked as follows with $m = 2$, $n = 15$, and $q = p = 8$. In particular, the linear basis series of $L_i(z^{-1})$, $i = 1, 2$, are selected as discrete-time Laguerre basis detailed in Appendix with $\varrho = 0.1$ and $T = 2$. Define a set of polynomial and trigonometric functions

$$\mathbb{G} = \{u^i, \sin(ju), \cos(ju) \mid i \in \{0, 1, 2, 3, 7\}, j \in \{1, \dots, 5\}\}.$$

The selection of the nonlinear functions $g_i(u)$, $i = 1, \dots, 15$, makes the complete set \mathbb{G} . The spatial basis functions are picked as polynomials

$$\psi(x) = \rho(x) = [1, x, \dots, x^7]^T.$$

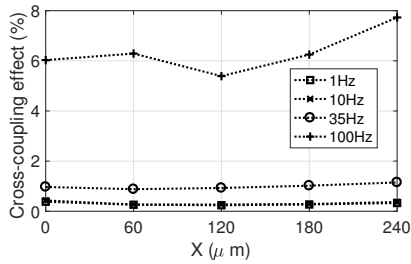


Fig. 5. The evolution of cross-coupling effect at different X - Y axes contacting positions $\{0, 60, 120, 180, 240\}$ μm along the increasing exciting frequency $\{1, 10, 35, 100\}$ Hz. Here, the cross-coupling effect is quantified as the percentage of cross-coupling magnitude to the exciting signal magnitude.

The Hammerstein channel number $N_c = 2$.

Take exciting frequency $f = 10$ Hz for example, in the first Hammerstein channel, with the aforementioned parameters, the evolution of the coefficient functions $a_i(x) = \psi^T(x)\eta_i^{(1)}$, $i = 1, \dots, 15$, along increasing position x are shown in Fig. 6. It is observed that the magnitudes of coefficients $\{a_1, a_2, a_6, a_{10}, a_{11}\}$ are much greater than the rest, which implies that the formers are more important than the latter. So, to reduce computational complexity and to avoid over-fitting, it suffices to cut off the unnecessary bases associated to those tiny coefficients. Analogously, the space-relevant coefficient functions $b_i(x) = \rho^T(x)\xi_i^{(1)}$, $i = 1, 2$ in the linear block $G(z^{-1}, x)$ of the first Hammerstein channel are shown in Fig. 7. The spatial distribution of the coefficients of both $N(\cdot, x)$ and $G(z^{-1}, x)$ is thus exhibited, which helps reveal the spatial evolution nature of the nonlinear cross-coupling dynamics.

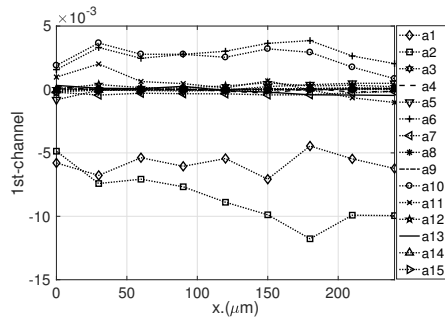


Fig. 6. Spatial-relevant coefficients $a_i(x)$, $i = 1, \dots, 15$, of the first Hammerstein channel of Eq. (9).

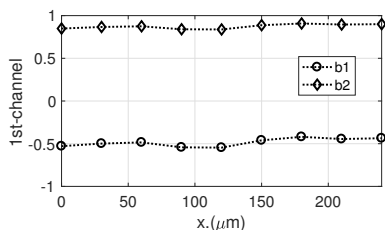


Fig. 7. Spatial-relevant coefficients $b_i(x)$, $i = 1, 2$, of the first Hammerstein model channel of (9).

The X -axis motional modeling performances of $\{0\mu\text{m}; 1\text{Hz}, \dots, 100\text{Hz}\}$ and $\{240\mu\text{m}; 1\text{Hz}, \dots, 100\text{Hz}\}$ are shown in Figs. 8 (a)–(h), respectively. Distinct cross-coupling hysteresis dynamics with different X -positions and exciting frequencies are observed. Again, along with increasing frequency, the cross-coupling effect is intensified, and the nonlinear modeling thus becomes more challenging. Quantitatively speaking, the average magnitude of $\{0\mu\text{m}; 1\text{Hz}, \dots, 100\text{Hz}\}$ and $\{240\mu\text{m}; 1\text{Hz}, \dots, 100\text{Hz}\}$ are $\{0.98, 1.02, 1.57, 1.36\}$ μm and $\{0.67, 0.80, 1.96, 1.97\}$ μm , respectively. To give a more vivid comparison of the modeling errors at different positions and exciting frequencies, we demonstrate the modeling errors at two contacting points $\{0\mu\text{m}, 240\mu\text{m}\}$ along increasing exciting frequencies $\{1\text{Hz}, 10\text{Hz}, 35\text{Hz}, 100\text{Hz}\}$. Evidently, the Hammerstein modeling error keeps at a low level (less than 8%), and the effectiveness of the modeling scheme is thus verified. Recall the PI stage resonant frequency of 140 Hz, we set the highest frequency of the exciting input signal as 100 Hz.

Next, to show the merits of the proposed distributed Hammerstein model, we consider Preisach model [13] as term of comparison in Fig. 8 as well. Due to its asymmetric hysteresis description [34], the modified Preisach model is given in a discrete form as

$$y(k) = p_1 u^3(k) + p_2 u(k) + \sum_{i=1}^n \alpha(r_i) \gamma_i[u(k)] + c, \quad (19)$$

where a third-degree polynomial $u(k) + u^3(k)$ is utilized to describe the asymmetric hysteresis, $\gamma_i[u(k)]$ is the play operator, $n = 10$ is picked as the number of the play operators, $\alpha(r_i) = \ell_i r_i$ is the weighted coefficient of the threshold $r_i = (i - 1)/n$, $i = 1, \dots, n$, and $[p_1, p_2, \alpha(r_1), \dots, \alpha(r_n), c]$ are the coefficient vector. Let $\Omega = [\Omega_1^T, \dots, \Omega_n^T]^T$ with $\Omega_k = [u(k)^3, u(k), \gamma_1[u(k)], \dots, \gamma_n[u(k)], 1]$, be the input vector, $Y = [y(1), \dots, y(n)]^T$ the output vector, and $X = [p_1, p_2, \alpha(r_1), \dots, \alpha(r_n), c]$ the coefficient vector, so $Y = \Omega X$. Accordingly, the estimated coefficient vector can be calculated as $\hat{X} = (\Omega^T \Omega)^{-1} \Omega^T Y$ by LSE [29].

Evidently, it is observed in Fig. 8 that the modeling error of the present Hammerstein model is much lower than that of the Preisach model. Meanwhile, with increasing exciting frequency, the modeling accuracy advantage of Hammerstein model is intensified. To show the result more vividly, we exhibit the modeling errors of the two models, respectively, in frequency domain in Fig. 9 with $f = 10$ Hz. It is observed that the modeling error e of the proposed Hammerstein model is much lower than that of the Preisach model within the entire bandwidth of $[0, 300]$ Hz, especially within the bandwidth of $[25, 100]$ Hz. To make a quantitative comparison between the two models, we exhibit the modeling errors of the Hammerstein and Preisach models in Fig. 10 with different exciting frequencies and X - Y axes contacting positions. Therein, compared with the Preisach model, the average modeling error of the Hammerstein model with exciting frequency $f = \{1, 10, 35, 100\}$ Hz, has been decreased by $\{52\%, 62\%, 74\%, 55\%\}$, respectively. Especially, the scenarios of 1 Hz and 100 Hz are shown in Figs. 10(a) and (b), respectively. Here, the

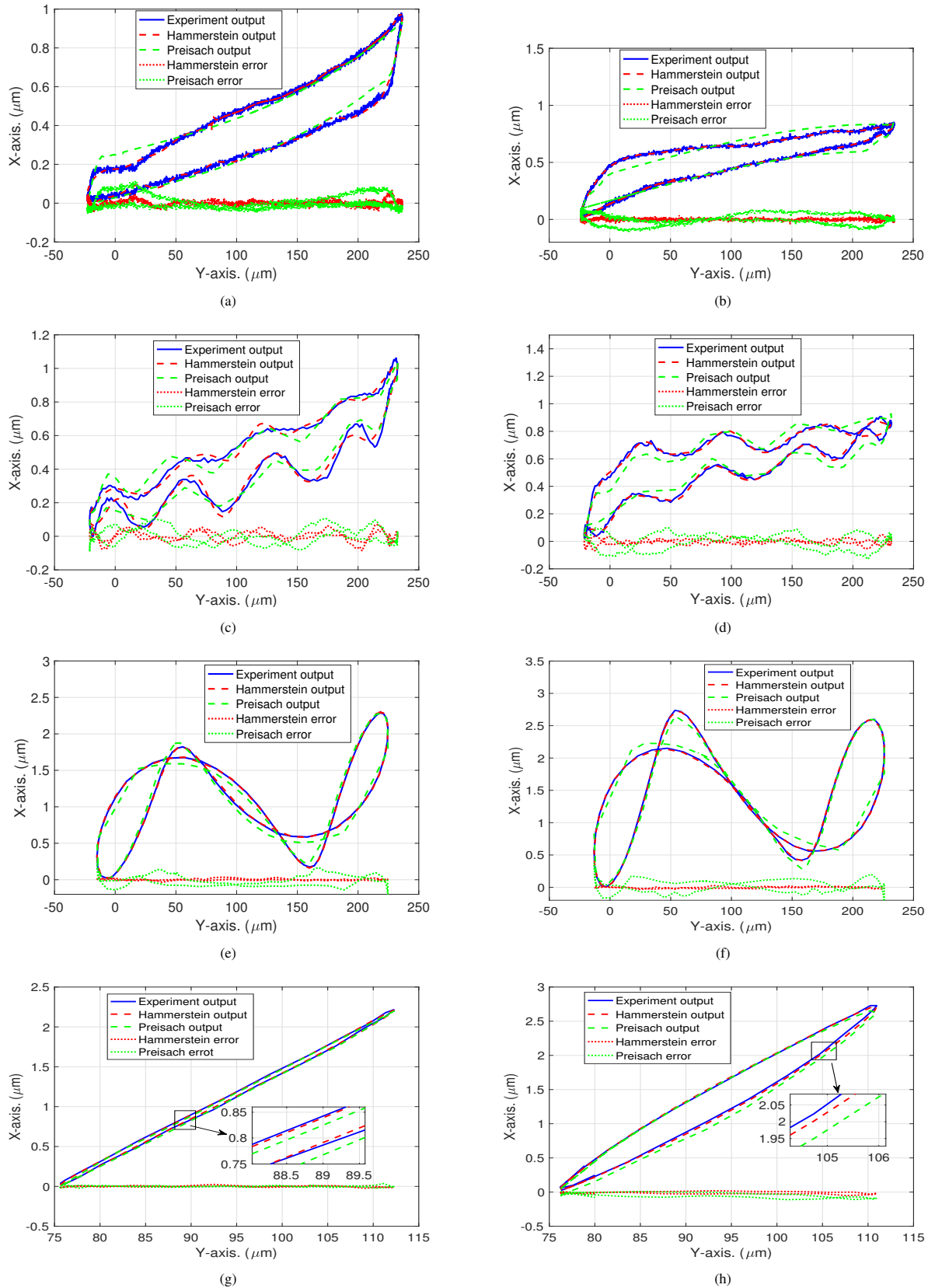


Fig. 8. The modeling performances at X - Y axes contacting positions of $x = 0 \mu\text{m}$ and $x = 240 \mu\text{m}$ with 1Hz exciting signal are shown in (a) and (b), with 10Hz in (c) and (d), with 35Hz in (e) and (f), and with 100Hz in (g) and (h), respectively.

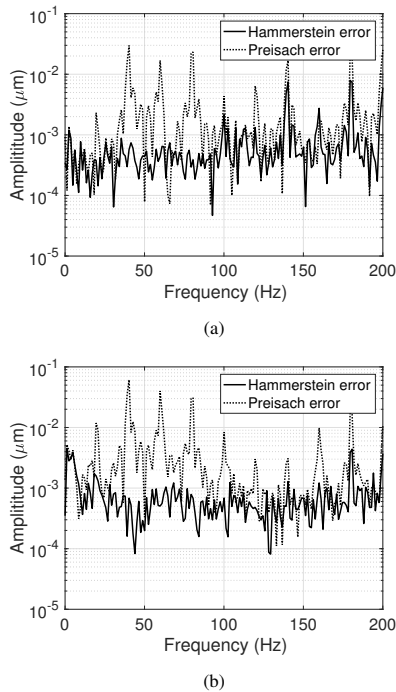


Fig. 9. The spectrum comparison of modeling errors at X–Y axes contacting positions of $x = 0$ and $240\mu\text{m}$ with $f = 10\text{Hz}$ exciting signal are shown in (a) and (b), corresponding to Fig. 8 (c) and (d), respectively.

modeling error is calculated as $e(t, x) := \frac{y(t, x) - y_m(t, x)}{y_{\max}(t, x) - y_{\min}(t, x)}$, the average modeling error $e(x)$ is the average of $e(t, x)$ over time t , and the average modeling error e at each exciting frequency f is the average of $e(x)$ over positions x . The effectiveness and superiority of the presented distributed Hammerstein method are thus verified. The advantage of the proposed Hammerstein model lies in its approximating capacity of both the nonlinearity and the spatial distribution of the cross-coupling effect. Note that, since the Preisach model does not effectively work with exciting frequency $f = 35\text{Hz}$, we just show the modeling curve of Hammerstein model in Figs. 8(e) and (f). Moreover, since inter-axis friction is intensified along rising excitation signal frequency, the coupling effect increases as well. Besides, the 100Hz coupling hysteresis in Figs. 8(g) and (h) are more symmetric than the 1Hz one in Figs. 8(a) and (b). Due to the symmetry of the Preisach operators, the modeling errors of the former is smaller than the latter. It is still worth mentioning that, to avoid over/less fitting, the series lengths of both linear and nonlinear blocks should be tuned according to the real sampling data.

To put the cross-coupling investigation into a more general scenario, we demonstrate the spatial/temporal evolution of the cross-coupling along increasing spatial variable x and temporal variable t in Fig. 11. Therein, we use an exciting input signal $u(t) = 4 + 5\sin(2\pi ft)$ V with $f = 1$ and 100Hz, respectively. It is observed that the modeling error of the distributed Hammerstein model ($\leq 8\%$ for $f = 1\text{Hz}$, and $\leq 2.2\%$ for $f = 100\text{Hz}$) is much less than that of the Preisach model ($\leq 13\%$ for $f = 1\text{Hz}$, and $\leq 3.8\%$ for $f = 100\text{Hz}$). The general virtue of the proposed distributed Hammerstein

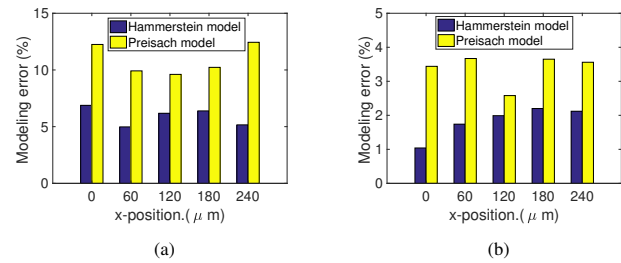


Fig. 10. Modeling errors of distributed Hammerstein model and Preisach model at different X–Y axes contacting positions with 1Hz exciting input signal are shown in (a), and with 100Hz in (b), respectively.

model is thus further verified.

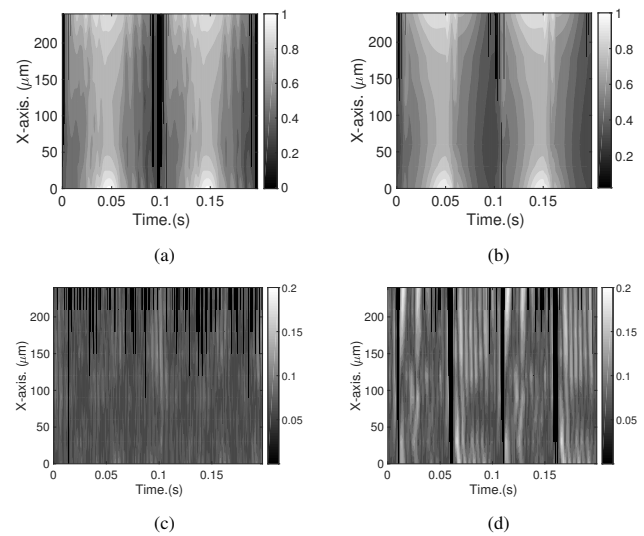


Fig. 11. (a),(b): Output heat maps of the Hammerstein and Preisach models of the cross-coupling effect, respectively; (c),(d) Error heat maps of the Hammerstein and Preisach models, respectively.

V. CONCLUSION

Cross-coupling has non-negligible adverse effects on the positioning control precision of multi-axis piezoelectric micropositioning stages, which hinders their further applications to nano-precision detection and manufacturing systems. In this paper, a distributed multi-channel Hammerstein model is proposed to approximate the spatial/temporal evolution of the nonlinear dynamics of the cross-coupling hysteresis. Theoretical analysis is provided to guarantee the convergence and modeling accuracy of the proposed distributed Hammerstein model. Finally, extensive modeling experiments are conducted to show its feasibility and superiority.

APPENDIX

The selection of $L(z^{-1}) = [L_1(z^{-1})^T, \dots, L_m(z^{-1})^T]^T$ follows the Laguerre functions given in [35], [36]. A slight abuse of notation of mixing time domain signals and frequency domain transfer function is used in Section III. Indeed, the

real implementation of $\zeta(t) = L(z^{-1})\mu(t)$ is given by the following dynamic equation in time domain,

$$\zeta(t+1) = A\zeta(t) + B\mu(t)$$

where, for two parameters ϱ and T ,

$$A = \begin{bmatrix} \rho_1 & 0 & \cdots & 0 \\ \frac{-\rho_1\rho_2-\rho_3}{T} & \rho_1 & \cdots & 0 \\ \vdots & \ddots & \ddots & \vdots \\ \frac{(-1)^{m-1}\rho_2^{m-2}(\rho_1\rho_2+\rho_3)}{T^{m-1}} & \cdots & \frac{-\rho_1\rho_2-\rho_3}{T} & \rho_1 \end{bmatrix}$$

$$B = \begin{bmatrix} \rho_4 & (-\frac{\rho_2}{T})\rho_4 & \cdots & (-\frac{\rho_2}{T})^{m-1}\rho_4 \end{bmatrix}^T$$

and

$$\rho_1 = \exp(-\varrho T), \rho_2 = T + \frac{2}{\varrho}(\rho_1 - 1),$$

$$\rho_3 = -T\rho_1 - \frac{2}{\varrho}(\rho_1 - 1), \rho_4 = \sqrt{2p} \frac{1 - \rho_1}{\varrho}.$$

REFERENCES

[1] G. Binnig and H. Rohrer. Scanning tunneling microscopy. *Surface Science*, 126(1-3):236–244, 1983.

[2] G. Binnig, C. F. Quate, and C. Gerber. Atomic force microscope. *Physical Review Letters*, 56(9):930, 1986.

[3] A. Tay, W. K. Ho, and X. Wu. Real-time control of photoresist extinction coefficient uniformity in the microlithography process. *IEEE Transactions on Control Systems Technology*, 15(1):99–105, 2007.

[4] Y. Yamagata and T. Higuchi. Ultrahigh vacuum precise positioning device utilizing rapid deformations of piezoelectric elements. *Journal of Vacuum Science and Technology*, 1(8):89–91, 1990.

[5] R. Fukui, A. Torii, and A. Ueda. Robot actuated by rapid deformation of piezoelectric elements. In *Proc. International Symposium on Micromechanics and Human Science*, pages 117–122, 2001.

[6] G.-Y. Gu, L.-M. Zhu, C.-Y. Su, H. D, and S. Fatikow. Modeling and control of piezo-actuated nanopositioning stages: a survey. *IEEE Transactions on Automation Science and Engineering*, 13(1):313–332, 2016.

[7] Y. K. Yong, S. R. Moheimani, B. J. Kenton, and K. K. Leang. High-speed flexure-guided nanopositioning: Mechanical design and control issues. *Review of Scientific Instruments*, 83(12):121101, 2012.

[8] S. Karunanidhi and M. Singaperumal. Design, analysis and simulation of magnetostrictive actuator and its application to high dynamic servo valve. *Sensors and Actuators A: Physical*, 157(2):185–197, 2010.

[9] Y. K. Yong, K. Liu, and S. O. R. Moheimani. Reducing cross-coupling in a compliant XY nanopositioner for fast and accurate raster scanning. *IEEE Transactions on Control Systems Technology*, 18(5):1172–1179, 2010.

[10] Y. Sun and J. H. L. Pang. AFM image reconstruction for deformation measurements by digital image correlation. *Nanotechnology*, 17(4):933, 2006.

[11] Habibullah, H. R. Pota, I. R. Petersen, and M. S. Rana. Creep, hysteresis, and cross-coupling reduction in the high-precision positioning of the piezoelectric scanner stage of an atomic force microscope. *IEEE Transactions on Nanotechnology*, 12(6):1125–1134, 2013.

[12] O. M. El Rifai and K. Youcef-Toumi. Coupling in piezoelectric tube scanners used in scanning probe microscopes. In *Proc. Amer. Control Conf.*, volume 4, pages 3251–3255, 2001.

[13] P. Ge and M. Jouaneh. Generalized preisach model for hysteresis nonlinearity of piezoceramic actuators. *Precision Engineering*, 20(2):99–111, 1997.

[14] R. Bouc. Forced vibration of mechanical systems with hysteresis. In *Proc. Conf. Nonlinear Oscillation, Prague*, pages 32–39, 1967.

[15] M. Goldfarb and N. Celanovic. Modeling piezoelectric stack actuators for control of micromanipulation. *IEEE Transactions on Control Systems Technology*, 17(3):69–79, 1997.

[16] J.-W. Wu, J.-J. Chen, M.-L. Chiang, J.-T. Yu, and L.-C. Fu. Design and control of phase-detection mode atomic force microscopy for reconstruction of cell contours in three dimensions. *IEEE Transactions on Nanotechnology*, 13(4):639–649, 2014.

[17] M. S. Rana, H. R. Pota, and I. R. Petersen. Nonlinearity effects reduction of an afm piezoelectric tube scanner using mimo mpc. *IEEE/ASME Transactions on Mechatronics*, 20(3):1458–1469, 2015.

[18] Y.-Q. Xie, Y.-H. Tan, and R.-L. Dong. Nonlinear modeling and decoupling control of XY micropositioning stages with piezoelectric actuators. *IEEE/ASME Transactions on Mechatronics*, 18(3):821–832, 2013.

[19] Y.-D. Qin, B. Shirinzadeh, Y.-L. Tian, L. Yan, D.-W. Zhang, and U. Bhagat. Design and computational optimization of a decoupled 2-DOF monolithic mechanism. *IEEE/ASME Transactions on Mechatronics*, 19(3):872–881, 2014.

[20] U. Bhagat, B. Shirinzadeh, L. Clark, Y.-D. Qin, Y.-L. Tian, and D.-W. Zhang. Experimental investigation of robust motion tracking control for a 2-DOF flexure-based mechanism. *IEEE/ASME Transactions on Mechatronics*, 19(6):1737–1745, 2014.

[21] R.-F. Fung, Y.-L. Hsu, and M.-S. Huang. System identification of a dual-stage XY precision positioning table. *Precision Engineering*, 33:71–80, 2009.

[22] S. K. Das, H. R. Pota, and I. R. Petersen. Multivariable negative-imaginary controller design for damping and cross coupling reduction of nanopositioners: A reference model matching approach. *IEEE/ASME Transactions on Mechatronics*, 20(6):3123–3134, 2015.

[23] Q. Xu. Identification and compensation of piezoelectric hysteresis without modeling hysteresis inverse. *IEEE Transactions on Industrial Electronics*, 60(9):3927–3937, 2013.

[24] C. Qi, H.-T. Zhang, and H.-X. Li. A multi-channel spatio-temporal Hammerstein modeling approach for nonlinear distributed parameter processes. *Journal of Process Control*, 19:85–99, 2009.

[25] C.-X. Li, G.-Y. Gu, M.-J. Yang, and L.-M. Zhu. Design, analysis and testing of a parallel-kinematic high-bandwidth XY nanopositioning stage. *Review of Scientific Instruments*, 84(12):125111, 2013.

[26] L.-J. Lai, G.-Y. Gu, and L.-M. Zhu. Design and control of a decoupled two degree of freedom translational parallel micro-positioning stage. *Review of Scientific Instruments*, 83(4):045105, 2012.

[27] P. Duren. *Theory of Hp-Spaces*. New York: Academic Press, 1970.

[28] G. H. Golub and C. F. Van Loan. *Matrix Computations*. The Johns Hopkins University Press, 3rd edition, 1996.

[29] L. Ljung. *System Identification*. Englewood Cliffs, NJ: Prentice-Hall, 2nd edition, 1999.

[30] Y. Li and Q. Xu. Design and analysis of a totally decoupled flexure-based XY parallel micromanipulator. *IEEE Transactions on Robotics*, 25(3):645–657, 2009.

[31] G. Schitter, P. J. Thurner, and P. K. Hansma. Design and input-shaping control of a novel scanner for high-speed atomic force microscopy. *Mechatronics*, 5–6:282–288, 2008.

[32] G.-Y. Gu, C.-X. Li, L.-M. Zhu, and C.-Y. Su. Modeling and identification of piezoelectric-actuated stages cascading hysteresis nonlinearity with linear dynamics. *IEEE/ASME Transactions on Mechatronics*, 21(3):1792–1797, 2016.

[33] C.-X. Li, G.-Y. Gu, L.-M. Zhu, and C.-Y. Su. Odd-harmonic repetitive control for high-speed raster scanning of piezo-actuated nanopositioning stages with hysteresis nonlinearity. *Sensors & Actuators: A. Physical*, 244:95–105, 2016.

[34] G.-Y. Gu, L.-M. Zhu, and C.-Y. Su. Modeling and compensation of asymmetric hysteresis nonlinearity for piezoceramic actuators with a modified Prandtl-Ishlinskii model. *IEEE Transactions on Industrial Electronics*, 61(3):1583–1595, 2014.

[35] C. C. Zervos and G. A. Dumont. Deterministic adaptive control based on laguerre series representation. *International Journal of Control*, 48(6):2333–2359, 1988.

[36] G. A. Dumont, C. C. Zervos, and G. L. Pageau. Laguerre-based adaptive control of pH in an industrial bleach plant extraction stage. *Automatica*, 4(781–787), 26.



Hai-Tao Zhang (M’07–SM’13) received the B.E. and Ph.D. degrees from the University of Science and Technology of China, Hefei, China, in 2000 and 2005, respectively. During January–December 2007, he was a Postdoctoral Researcher with the University of Cambridge, Cambridge, U.K. Since 2005, he has been with Huazhong University of Science and Technology, Wuhan, China, where he was an associate professor from 2005 to 2010 and has been a full professor since 2010. His research interests include swarming intelligence, model predictive control, and multi-agent systems control. He is an associate editor of *IEEE Transactions on Circuits and Systems II* and *Asian Journal of Control*.



Bo Hu received his Bachelor's degree from Hefei University of Technology in 2015 and got his Master's degree of Engineering from Huazhong University of Science and Technology in 2017. His research interests focused on nonlinear hysteresis modeling and control.



Xiang Huang received the B.S. degree from Wuhan University of Science and Technology, Wuhan, China, in 2015. He is currently working toward the Ph.D. degree at the School of Automation, Huazhong University of Science and Technology, Wuhan, China. His research interests include modeling and control of hysteresis.



Linlin Li received the B.E. degree (with honors) in Mechanical design, manufacturing and automation from Shandong University, Jinan, China, in 2014. She is currently working toward the Ph.D. degree in mechanical engineering at Shanghai Jiao Tong University, Shanghai, China. Her research interests include mechatronics, modeling and control of high-bandwidth nanopositioning stages and Atomic Force Microscope.



Zhiyong Chen (S'03-SM'13) received the B.E. degree from the University of Science and Technology of China, and the M.Phil. and Ph.D. degrees from the Chinese University of Hong Kong, in 2000, 2002 and 2005, respectively. He worked as a research associate at the University of Virginia during 2005-2006. He joined the University of Newcastle, Australia, in 2006, where he is currently a professor. He is also a Cheung Kong Chair Professor with Central South University, Changsha, China. His research interests include nonlinear systems and control, biological systems, and multi-agent systems. He is/was an associate editor of *Automatica*, *IEEE Transactions on Automatic Control* and *IEEE Transactions on Cybernetics*.

ological systems, and multi-agent systems. He is/was an associate editor of *Automatica*, *IEEE Transactions on Automatic Control* and *IEEE Transactions on Cybernetics*.



Guoying Gu (S'10-M'13) received the B.E. and Ph.D. degrees from Shanghai Jiao Tong University, Shanghai, China, in 2006 and 2012, respectively. Since October 2012, he has worked at Shanghai Jiao Tong University, where he is currently a professor. He was as a Humboldt Postdoc Fellow at University of Oldenburg, Oldenburg, Germany. He was a Visiting Scholar at Massachusetts Institute of Technology, National University of Singapore and Concordia University. His research interests include soft robotics, bioinspired robot design and motion control, smart materials actuators and sensors, and additive manufacturing with soft materials. He is the winner of multiple awards including Young Cheung Kong Scholar of the Chinese Ministry of Education, National Science Fund for Excellent Young Scholars, the first prize of natural science of Ministry of Education. Now he serves as Associate Editor of *International Journal of Advanced Robotic Systems*.

control, smart materials actuators and sensors, and additive manufacturing with soft materials. He is the winner of multiple awards including Young Cheung Kong Scholar of the Chinese Ministry of Education, National Science Fund for Excellent Young Scholars, the first prize of natural science of Ministry of Education. Now he serves as Associate Editor of *International Journal of Advanced Robotic Systems*.



Dongrui Wu (S'05-M'09-SM'14) received the PhD degree in electrical engineering from the University of Southern California in 2009. He was a Lead Researcher at GE Global Research, and Chief Scientist of several startups. He is now a professor in the School of Automation, Huazhong University of Science and Technology, Wuhan, China. His research interests include affective computing, brain-computer interface, computational intelligence, and machine learning. He received the IEEE CIS Outstanding PhD Dissertation Award in 2012, the *IEEE Transactions on Fuzzy Systems* outstanding paper award in 2014. He is an associate editor of *IEEE Transactions on Fuzzy Systems*, *IEEE Transactions on Human-Machine Systems*, and *IEEE Computational Intelligence Magazine*.

Transactions on Fuzzy Systems outstanding paper award in 2014. He is an associate editor of *IEEE Transactions on Fuzzy Systems*, *IEEE Transactions on Human-Machine Systems*, and *IEEE Computational Intelligence Magazine*.



Ye Yuan (M'13) received the B.Eng. degree (Valedictorian) from the Department of Automation, Shanghai Jiao Tong University, Shanghai, China, in 2008, and the M.Phil. and Ph.D. degrees from the Department of Engineering, University of Cambridge, Cambridge, U.K., in 2009 and 2012, respectively. He has been a Full Professor at the Huazhong University of Science and Technology, Wuhan, China since 2016. Prior to this, he was a Postdoctoral Researcher at UC Berkeley, a Junior Research Fellow at Darwin College, University of

Cambridge. His research interests include system identification and control with applications to cyber-physical systems.



Bowen Xu received his B.S. degree from Xidian University, Xi'an, China, in 2016. He is currently working toward the Ph.D degree in School of Automation, Huazhong University of Science and Technology, Wuhan, China. He was an outstanding reviewer of *Asian Journal of Control* in 2017. His research interests include multi-agent systems control.